

An Experimental and Computational Study of Aerodynamic Properties of Rugby Balls

¹FIROZ ALAM, ¹ALEKSANDAR SUBIC, ¹SIMON WATKINS, ²JAMAL NASER and ³M.G. RASUL

¹School of Aerospace, Mechanical and Manufacturing Engineering, RMIT University, AUSTRALIA

²Faculty of Engineering and Industrial Sciences, Swinburne University of Technology, AUSTRALIA

³Faculty of Sciences, Engineering and Health, Central Queensland University, AUSTRALIA

Corresponding author: firoz.alam@rmit.edu.au

Abstract: The aerodynamic properties of rugby balls as a function of wind speeds and yaw angles were measured using experimental and computational methods. The average drag and side forces coefficients for all speeds and yaw angles were computed and compared. The flow pattern around the rugby ball was visualized using wool tuft and smoke. No significant variation in Reynolds numbers was found in CFD results, however, some variations were noted in experimental findings. The average drag coefficient of a rugby ball at zero yaw was 0.18 and 0.14 in experimental and computational studies and this rose to about 0.60 and 0.50 when yawed at 90 degrees respectively.

Key-Words: Drag coefficient, side force, wind tunnel, EFD, CFD

1 Introduction

Aerodynamic properties of a sporting ball play a significant role as they influence the speed, motion, trajectory and ultimately place of landing of the ball. Aerodynamics of various sports balls have been widely studied by Alam *et al.* [1-6], Mehta [7], Mehta and Pallis [8], Sayers and Hill [9], Smits and Oggo [10] and Wilkinson [11]. Despite the popularity of games such as Rugby, there appears to be scant aerodynamic research in the area. In the recent World Rugby Cup it was clearly evident that distance kicking plays an increasingly significant role in the outcome of the game. The crosswind and spin have significant effects on ball's flight trajectory and sideway deviation. Understanding of these will enhance significantly the performance of the game. Although the rugby game is widely played around the world, very limited studies have been conducted and reported to the open literature. Prior aerodynamic studies on rugby balls have been reported to the open literature by Alam *et al.* [1-4] and Seo *et al.* [12]. Most of these works were (except Alam *et al.* [3]) are experimental. Computational Fluid Dynamics (CFD) method nowadays has been widely used in aerodynamics and fluid mechanics applications, thanks to the advancement of computational power. Using CFD method, it is sometime easier to visualize a complex flow phenomenon and shorten design cycles and market faster. Although CFD is faster and cost effective, it is not a complete replacement of experimental validation. Therefore, the CFD method can be used to supplement the Experimental

Fluid Dynamics (EFD) findings and most cases needs to be validated by EFD method. As no prior study by CFD method on rugby ball aerodynamics has been reported to the public domain, a CFD study on rugby ball aerodynamics seems to be timely. Therefore, the primary objective of this work was to study the aerodynamic properties (such as drag and side force) of a rugby ball using CFD method and compare the results with EFD findings. Ultimately the work will be extended to understanding the complexities of spinning rugby ball but here it is restricted to non-spinning flight.

The aerodynamic drag, lift and side force are directly related to air velocity, cross sectional area of the ball, air density and air viscosity. Drag, lift and side forces are generally defined in fluid mechanics as:

$$D = C_D \frac{1}{2} \rho V^2 A \quad (1)$$

$$L = C_L \frac{1}{2} \rho V^2 A \quad (2)$$

$$S = C_S \frac{1}{2} \rho V^2 A \quad (3)$$

Where C_D , C_L and C_S are the non-dimensional drag, lift and side force coefficients respectively, ρ is the air density (kg/m^3), V is the free stream air velocity (m/s), and A is the cross sectional area of the ball (m^2).

The non-dimensional C_D , C_L and C_S are defined as:

$$C_D = \frac{D}{\frac{1}{2} \rho V^2 A} \quad (4)$$

$$C_L = \frac{L}{\frac{1}{2} \rho V^2 A} \quad (5)$$

$$C_S = \frac{S}{\frac{1}{2} \rho V^2 A} \quad (6)$$

The C_D , C_L , C_S are related to the non-dimensional parameter, Reynolds number (Re), and defined as:

$$Re = \frac{\rho V D}{\mu} \quad (7)$$

2 Experimental Procedure

2.1 Experimental Facilities and Equipment

The experimental study (EFD) was conducted in RMIT Industrial Wind Tunnel. The wind tunnel is a closed return circuit with a turntable to yaw suitably sized objects. The maximum speed of the free stream velocity in the tunnel's test section is approximately 145 km/h. The tunnel has rectangular test section dimension, which is 3 m (wide) x 2 m (high) x 9 m (long). A plan view of the tunnel is shown in Fig. 1. The tunnel was calibrated before conducting the experiments. The tunnel's air speeds were measured via a modified NPL (National Physical Laboratory) ellipsoidal head Pitot-static tube (located at the entry of the test section, see Fig. 2) connected to a MKS Baratron pressure sensor through flexible tubing. Purpose made computer software was used to compute all 6 forces and moments (drag, side, lift forces, and yaw, pitch and roll moments) and their non-dimensional coefficients. A mounting stud was manufactured to hold the ball and was mounted on a six component force sensor (type JR-3). The JR-3 force sensor allows loading at the sensor's location. It is relatively simple to use for the collection of data by defining the loads applied to the sensor in 6 degrees of freedom. Thanks to its high stiffness and integration into the system, the sensor allows minimal degradation of system dynamics, positioning accuracy, and high resonant frequency, allowing accurate sensor response to rapid force changes.

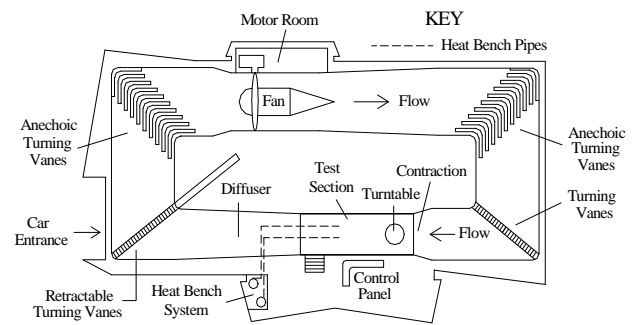


Fig. 1: A Plan View of RMIT Industrial Wind Tunnel (Alam [4])

2.2 Description of the Rugby Ball

A new rugby ball made by SUMMIT Australia was selected for the experimental work as it is officially used in various tournaments in Australia. The external dimensions of the rugby ball were 280 mm in length and 184 mm in diameter. The ball was made of four synthetic rubber segments (see Fig. 3). The rugby ball was tested in the wind tunnel under a range of wind speeds (40 km/h to 140 km/h with an increment of 20 km/h) at yaw angles $\pm 90^\circ$ with an increment of 10° .



Fig. 2: Experimental set up in RMIT Industrial Wind tunnel with a Rugby ball

Figures 2 and 3 show the experimental set up of the rugby ball in the wind-tunnel test section. The distance between the bottom edge of the ball and the tunnel floor was 350 mm, which is well above the tunnel's boundary layer and considered to be out of ground effect. During the measurement of forces and moments, the tare forces were removed by measuring the forces on the sting in isolation and then removing them from the force of the ball and sting. Since the blockage ratio was extremely low no corrections were made.

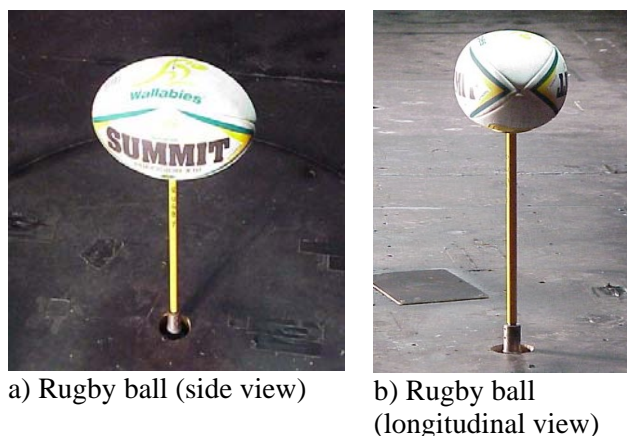


Fig. 3: A view of typical rugby ball

3 CFD Model Development and Computational Procedure

Simplified rugby ball with four segments was developed by using Solid Works®. The smooth oval shape was achieved by joining all four equal size segments. The joint between the two segments possesses a seam to replicate the real ball. The model is shown in Fig. 4. The model's dimensions are: length- 280 mm, width (diameter)- 184 mm and seam radius-2 mm. The simplified model was imported to GAMBIT, a pre-processor of CFD code FLUENT. In CFD modelling FLUENT 6.1 was used.

In this study, the turbulence model 'k-epsilon' was used. The model is based on the RANS (Reynolds Average Navier Stokes) equations as complete time dependent solution of the full Navier Stokes equations is difficult to obtain with current computational power. The RANS equations calculate the mean flow quantities which greatly reduce the computational time. For steady mean flow, there is no time derivative in the governing equations and a steady state solution with minimum cost and computational power can be obtained. The Reynolds Average Navier-Stokes equations used in this study can be written in Cartesian Tensor form in equations 8 and 9.

$$\frac{\partial \rho}{\partial t} + \frac{\partial}{\partial x_i} (\rho u_i) = 0 \quad (8)$$

$$\frac{\partial}{\partial t} (\rho u_i) + \frac{\partial}{\partial x_j} (\rho u_i u_j) = -\frac{\partial \rho}{\partial x_i} + \frac{\partial}{\partial x_j} \left[\mu \left(\frac{\partial u_i}{\partial x_j} + \frac{\partial u_j}{\partial x_i} - \frac{2}{3} \delta_{ij} \frac{\partial u_l}{\partial x_l} \right) \right] + \frac{\partial}{\partial x_j} (-\rho \bar{u}_i \bar{u}_j) = 0 \quad (9)$$

The RANS equation above is the same form as full Navier-Stokes equations. The velocities and other

solution variables in these equations are time averaged value.

A wind tunnel with reduced dimension (in order to reduce computational time) was created using GAMBIT. The reduced tunnel's dimensions are: length- 2500 mm, width- 2000 mm and height-2000 mm. After the creation of the volume for the wind tunnel, the volume of the rugby ball was subtracted from the volume of the wind tunnel and the area within the wind tunnel is empty. The size function was used to mesh the volume. The tetrahedron grid was used to mesh the ball. A total of 900,000 cells were required to mesh the model effectively. The quality of meshing was checked using skewness factor in GAMBIT. The finished meshed models are shown in Figs. 5 and 6. The finished mesh can be refined further in FLUENT software if requires. The boundary conditions for the modelling were: the frontal area of the wind tunnel was the velocity inlet as the wind source comes from there and the rear face area of the wind tunnel was the pressure outlet as the wind exits the test section from there. The rest of the boundary types were specified as walls including the rugby ball, which is also considered as wall. The boundary parameters are shown in Table 1. The accuracy of CFD solution is primarily governed by the number of cells in a grid, a larger number of cells equates to a better solution. However, an optimal solution can be achieved by using fine mesh at locations where the flow is very sensitive and relatively coarse mesh where airflow has little changes. As mentioned earlier, Tetrahedron mesh with mid-edged nodes was used in this study. Figure 5 shows a model of the rugby ball with the tetrahedron mesh. Generally, the structured (rectangular) mesh is preferable to tetrahedron mesh as it gives more accurate results. However, there are difficulties to use structured mesh in complex geometry. In this study, a total of seven simplified models were meshed with tetrahedron mesh. Seven models were constructed to simulate the yawed wind conditions (crosswinds effects) as only one model was used for each yawed condition. The control volume was modelled using GAMBIT. In order to use fine mesh in the interested areas, sizing function in GAMBIT was used. Mesh validation was done using Examining Mesh command or "Check Volume Meshes". A grid independency test was performed (see Figure 6a) and the above mentioned 900,000 cells appeared to give grid independent results. The Segregated (Implicit) solver was used for the computation as it is faster and produced results close to experimental findings. Additionally, the segregated implicit solver is widely used for incompressible and mildly

compressible flows. The flow was defined as inviscid, laminar and/or turbulent and as mentioned earlier, the k-epsilon model with enhanced wall treatment was used for the turbulence modelling. The non-equilibrium wall function was used as the flow is complex involving separation, re-attachment and impingement. Other model such as k-omega was also used to see the variation in solutions and results.

Table 1: CFD modelling boundary parameters

	Description	Boundary Conditions
1	Inlet	VELOCITY_INLET
2	Outlet	PRESSURE_OUTLET
3	Rugby Ball	WALL
4	Control Volume (Default Setting)	WALL

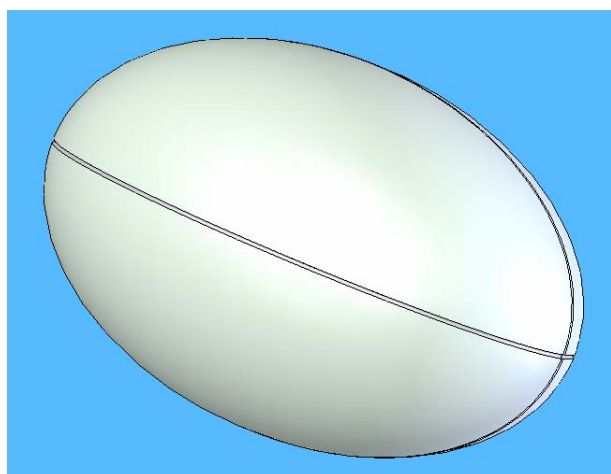


Fig. 4: Simplified CFD model of rugby ball

Velocity inlet boundary conditions were used to define flow velocity and turbulence at the flow inlet. Flow inlet velocities were from 40 km/h to 140 km/h with an increment of 20 km/h at ±90° yaw angles with an increment of 30° to compare the CFD modelling results with experimental findings. The direction of airflow was normal to the inlet and the reference frame was set as absolute for the velocity. In order to control the solution, the 2nd order upwind scheme interpolation was selected as the simulation involves Tri/tetrahedral meshes. After setting all corresponding parameters, the simulation was initialized and iterated, and the results were obtained. The convergence criterion for continuity equations was set as 1×10^{-5} (0.001%).

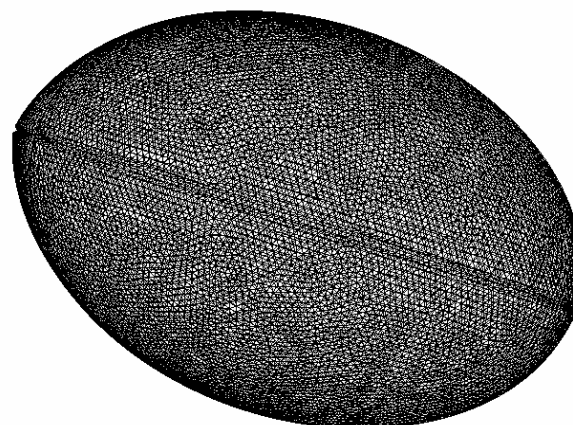


Fig. 5: Meshing of the rugby ball in CFD

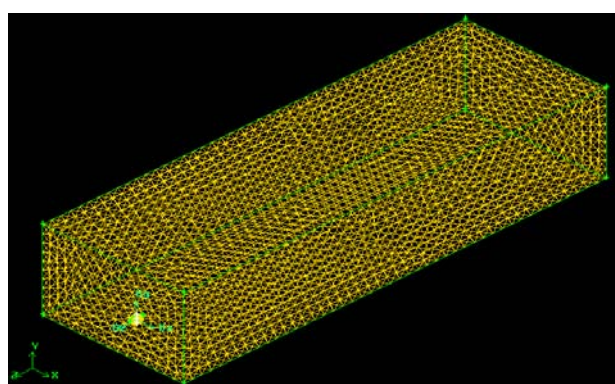


Fig. 6: Wind tunnel meshing in CFD

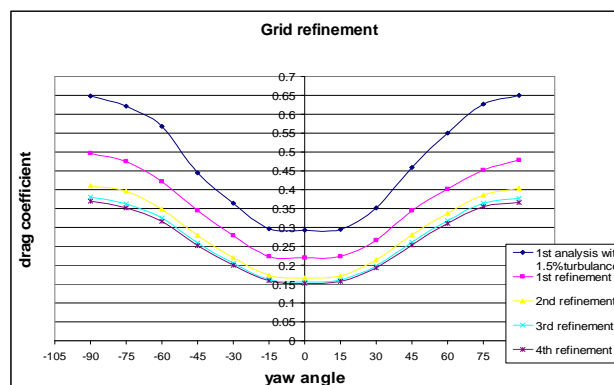


Fig. 6a: Cd variation with yaw angles as a function of grid optimisation

4 Results and Discussion

4.1 Experimental Results

The Rugby ball was tested at 40, 60, 80, 100, 120 and 140 km/h wind speeds under +100° to -80° yaw angles with an increment of 10°. Wool tufts and smoke were used to visualise the flow around the

ball at various yaw angles. The ball was yawed relative to the force sensor (which was fixed with its resolving axis along the mean flow direction whilst a ball was yawed above it) thus the wind axis system was employed. Flow visualisation by wool tufts at 0° and 90° yaw angles are shown in Figs. 7 and 8 respectively. The forces and moments were converted to non-dimensional parameters. The drag force coefficients and side force coefficients for 60 km/h to 140 km/h are plotted against yaw angles and shown in Figs. 9 and 10 respectively. A comparison of drag coefficients at all speeds and yaw angles for the rugby ball indicates that there is a slight lack of symmetry in the results (see Fig. 9). Whilst some errors arose from a slight lack of airflow and force balance symmetry, the errors are greater than expected. Examination of the ball indicated that the ball is not exactly symmetrical. The average drag coefficient of the rugby ball was experimentally found to be 0.18 at zero yaw angle. No significant variation in Reynolds numbers was evident at 90° yaw angle for the rugby ball except for the 60 km/h speed (see Fig. 9). With an increase in yaw angle, the drag coefficient increases due to a large and complex flow separation. Flow visualisation was conducted at 60, 100 and 140 km/h under ±90° yaw angles with an increment of 10° but is only given here for 60 km/h (see Figs. 7 and 8). Flow structures at 90° are complex. Flow separations start at approximately ¾ length from the front edge at zero yaw angles and the separations are complicated and time varying at 90° yaw angle.

The side force coefficients have minor off-set from 0° yaw angle for the rugby ball which is believed to be due to a small mounting error (Figure 10). A minor variation in Reynolds numbers was noted at the lowest Reynolds number (60 km/h). Significant variation in positive and negative magnitudes of side force coefficients with yaw angles was noted. The variation is believed to be due to asymmetric geometry of the ball.



Fig. 4: Flow structure around a rugby ball at 0° yaw angle

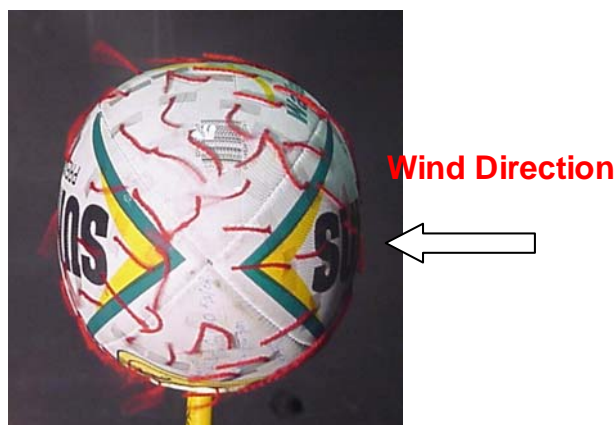


Fig. 8: Flow structure around a rugby at 90° yaw angle

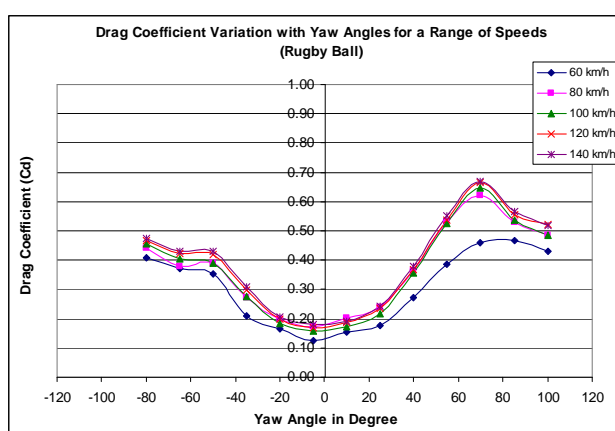


Fig. 9: Drag coefficients (C_D) as a function of yaw angles and wind speeds

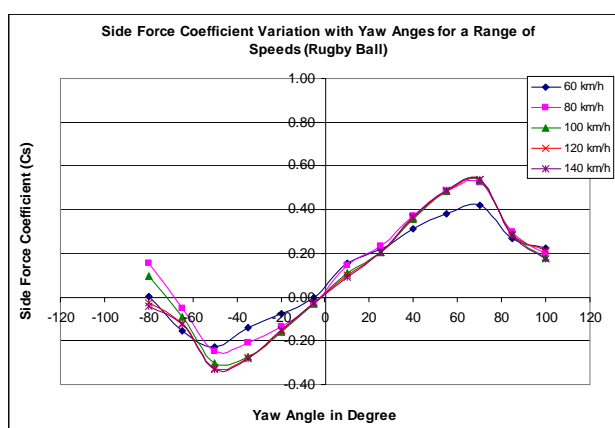


Fig. 10: Side force coefficients (C_S) as a function of yaw angles and wind speeds

4.2 Computational (CFD) Results

The CFD simulation was conducted using FLUENT 6.1 at a range of speeds (60 to 120 km/h with an increment of 20 km/h). The velocity vectors and static pressure distributions around the ball at 0° and 90° yaw angles for 100 km/h speed are shown in

Figs. 11 to 14. The drag coefficients (C_D) for 60 to 140 km/h with an increment of 20 km/h at $\pm 90^\circ$ yaw angles are shown in Figure 15. A significant variation in velocity vectors between 0° and 90° yaw angles is evident (see Figs. 11 and 12). At 0° yaw angle, the flow is more streamlined and attached compared to 90° yaw angle as expected. The velocity vectors are more chaotic in the leeward side of the ball (behind) at 90° compared to 0° yaw angles where the velocity vectors are relatively streamlined to the mean direction of the flow. The static pressure distribution pattern has similar trend like sphere. The highest negative pressure is noted at the lateral side at 90° yaw angle compared to 0° yaw angle (see Figs.13 & 14). However, a close inspection indicates that the pressure distributions are absolutely not symmetrical around the ball.

The drag coefficient and side force coefficient distribution as a function of yaw angles and wind speeds are shown in Figure 15 and 16 respectively. No significant Reynolds number variation was found in CFD analysis. The drag coefficients are almost independent of Reynolds numbers. The computed minimum drag coefficient at 0° yaw angles was approximately 0.14. However, the drag coefficient increases with an increase of yaw angles (see Fig. 15). The maximum drag coefficient was found at $\pm 90^\circ$ yaw angles (approximately 0.50). No significant asymmetry of drag coefficients between the positive and negative yaw angles was noted.

The side force coefficient demonstrates the highest magnitudes (0.25) at approximately $\pm 50^\circ$ yaw angles. As expected, zero side force coefficient was found at zero yaw angles.

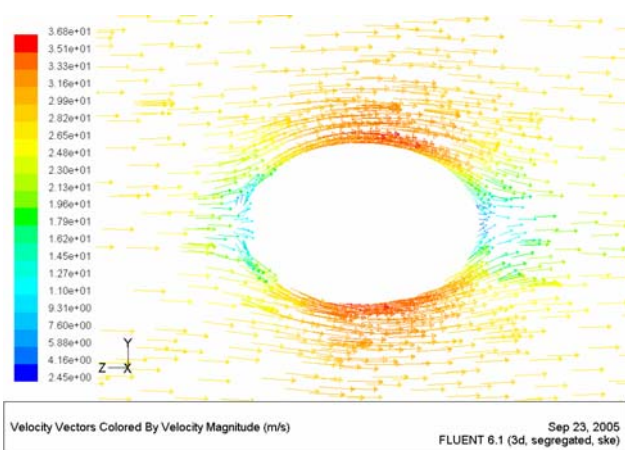


Fig. 11: Velocity vectors around the rugby ball at 0° yaw angle

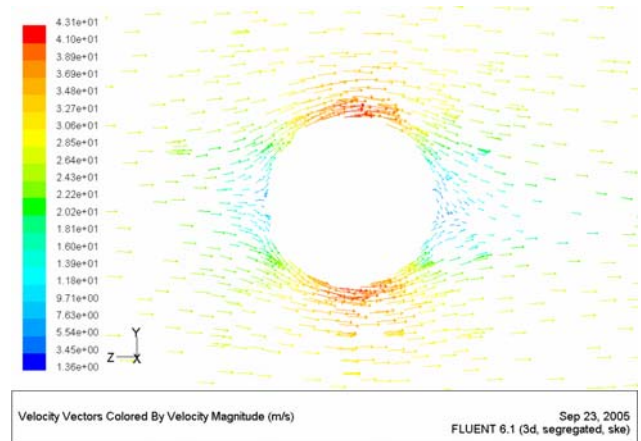


Fig. 12: Velocity vectors around the rugby ball at 90° yaw angle

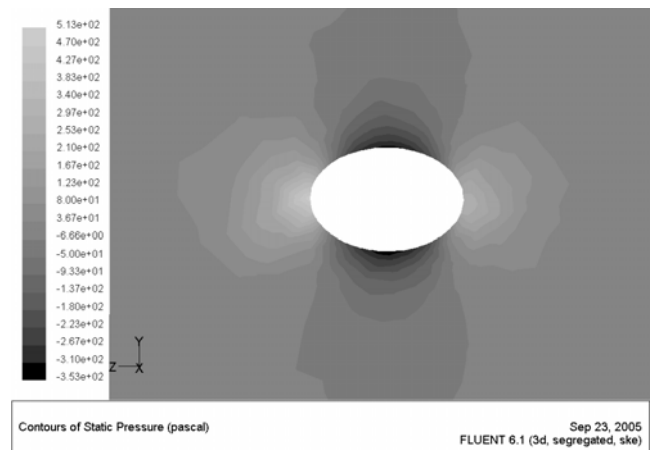


Fig. 13: Static pressure distribution around the rugby ball at 0° yaw angle

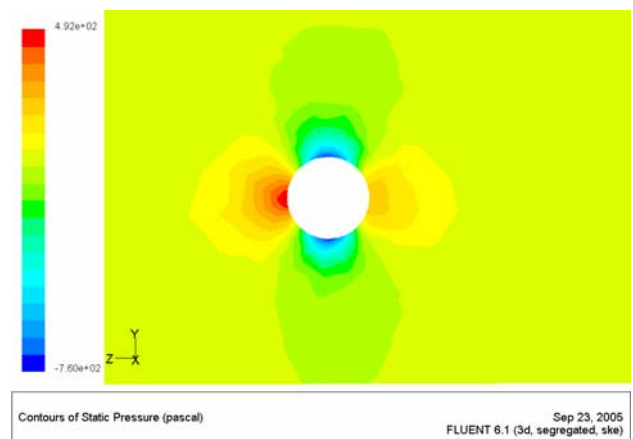


Fig. 14: Static pressure distribution around the rugby ball at 90° yaw angle

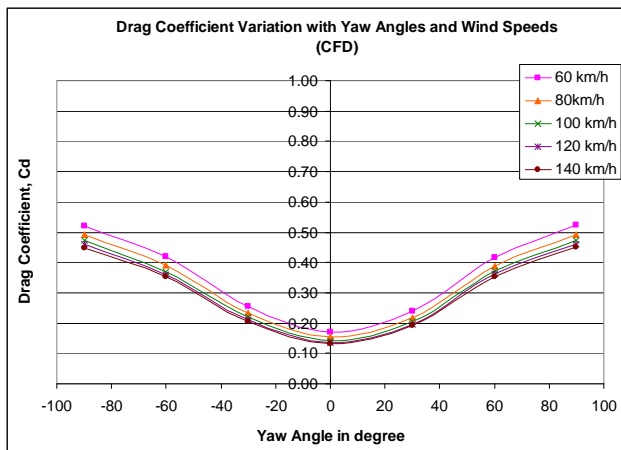


Fig. 15: Drag coefficients (C_D) as a function of yaw angles and wind speeds

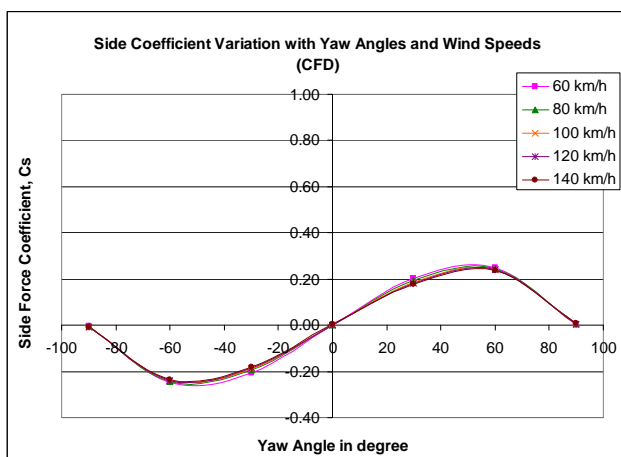


Fig. 16: Side force coefficients (C_s) as a function of yaw angles and wind speeds

4.3 Overall Discussion

The flow visualisation (with wool tuft and smoke) around the rugby ball indicated complex flow structures at 90° yaw angles (smoke flow visualisation pictures are not shown here). The similar flow pattern but lesser extent was also noted at 0° yaw angle. The separation was three dimensional in the leeward side of the ball. The experimentally determined drag coefficient (0.18 at 0° yaw angle and 0.60 at 90° yaw angle) is higher compared to computationally estimated drag coefficient (0.14 at 0° yaw angle and 0.50 at 90° yaw angle). The Reynolds number dependency was noted at 90° yaw angle in experimental analysis. However, a small variation at lower Reynolds numbers was noted in computational analysis.

A close inspection has revealed that the rugby ball is not fully symmetrical along the longitudinal axis. The ball surface was rough and was not fully oval shape as it was made of four segments. On the other hand, the simplified model in CFD analysis was fully symmetrical along the longitudinal and lateral axes. The surface was smooth and the flow was more uniform compared to the airflow in the wind tunnel. The cross sectional area was approximately circular compared to the real rugby ball. The cross sectional geometry of real rugby ball was slightly larger compared to a circular geometry of the CFD model.

The geometry of a real rugby ball is complex and hard to manufacture a parabolic 3D shape to perfection. However, the computational model used in this study was a perfectly symmetrical parabolic geometry. Using CFD, ideal theoretical results were generated. However, both CFD and experimental results have shown similar trends. In reality, the CFD results have significant variation from experimental results. These variations are believed to be due to over simplification of the model, inability to replicate real flow around the ball, limitation of CFD software and also mirror computational and experimental errors. Using the standard approximations formula, approximate error of 1.5% in forces coefficients was found both in experimental and computational studies, which can be considered within acceptable limits.

5 Conclusion

The following conclusions can be made from the work presented here:

- The aerodynamics resulting from the flight of irregular shaped sporting balls is extremely complex even when the ball is not spinning.
- The average drag coefficient for the rugby ball at zero yaw angles was found experimentally and computationally to be 0.18 and 0.14 respectively.
- The experimental and computational measurements indicated the average drag coefficient for the rugby ball at 90° yaw angles between 0.60 and 0.50 in experimental and computational studies respectively.
- The highest magnitude of side force coefficients for the rugby ball were found to be ± 0.25 at approximately 50° yaw angles in computational modeling. However, the highest positive side magnitude (+0.52) was noted at leeward side

yaw angles (+65°) and the highest negative magnitude (-0.35) was noted at windward side yaw angles (-50°).

- A significant variation in magnitudes of side force coefficients with yaw angles is believed to be due to asymmetry of the real rugby ball compared to the simplified CFD model.
- No significant Reynolds number variation of drag coefficients and side force coefficients was found in computational analysis. However, some variations were noted in experimental measurements.

6 Recommendation for Further Work

The following recommendations for future works can be made:

- Effects of spin on aerodynamic drag, lift and side force are important to investigate
- A comparative analysis of drag and side force coefficients for three major manufacturers' balls: Summit, Adidas and Gilbert is worthwhile to study

Acknowledgements

The authors express their sincere thanks to Mr Wisconsin Tio and Pek Chee We, School of Aerospace, Mechanical and Manufacturing Engineering, RMIT University for their extraordinary assistance with the CFD modelling of rugby balls.

References:

- [1] Alam, F., Subic, A. and Watkins, S. (2005), "Measurements of aerodynamic drag forces of a rugby ball and Australian Rules football" in *The Impact of Technology on Sport I* (edited by A. Subic and S. Ujihashi), Tokyo Institute of Technology, Japan, ISBN 0-646-45025-5, 12-16 September, pp 276-279.
- [2] Alam, F., Watkins, S. and Subic, A. (2004), "The aerodynamic drag of a rugby ball and Australian Rules football, *Proceedings of the 5th Bluff Body Aerodynamics and Applications (BBAA V) Conference*, 11-15 July, Ottawa, Canada, pp 211-214.
- [3] Alam, F., We, P. C., Subic, A. and Watkins, S. (2006), "A Comparison of Aerodynamic Drag of a Rugby Ball using EFD and CFD" in *The Engineering of Sport 6* (edited by E. F. Moritz and S. Haake), Vol. 2, ISBN 0-387-34678-3, Springer Science, Munich, Germany, pp. 145-150.
- [4] Alam, F., "The Effects of Car A-pillar and Windshield Geometry on Local Flow and Noise", PhD Thesis, Department of Mechanical and Manufacturing Engineering, RMIT University, 2000, Melbourne, Australia.
- [5] Alam, F., Watkins, S. and Subic, A. (2004), "The Aerodynamic Forces on a Series of Tennis Balls", *Proceedings of the 15th Australasian Fluid Mechanics Conference*, University of Sydney, 13-17 December, Sydney, Australia.
- [6] Alam, F., Subic, A. and Watkins, S. (2004), "Effects of Spin on Aerodynamic Properties of Tennis Balls" in *The Engineering of Sport 5*, Vol. 1, ISBN 0-9547861-0-6, pp 83-89, University of California, Davis, USA
- [7] Mehta, R. D. (1985), "Aerodynamics of Sports Balls", *Annual Review of Fluid Mechanics*, **17**, pp. 151-189.
- [8] Mehta, R. D. and Pallis, J. M. (2001b), "The aerodynamics of a tennis ball", *Sports Engineering*, **4**, No. 4, pp. 1-13.
- [9] Sayers, A. T. and Hill, A. (1999), "Aerodynamics of a cricket ball", *Journal of Wind Engineering and Industrial Aerodynamics*, **79**, No. 1-2, pp 169-182, January
- [10] Smits, A. J. and Ogg, S. (2004), "Golf ball aerodynamics", *The Engineering of Sport 5*, ISBN 0-9547861-0-6, pp 3-12.
- [11] Wilkinson, B. (1997), "*Cricket: The Bowler's Art*", Kangaroo Press, Australia, ISBN 0-86417-899-9, pp 1-191.
- [12] Seo, K., Kobayashi, O. and Murakami, M. (2004), "Regular and irregular motion of a rugby football during flight", *The Engineering of Sport 5*, ISBN 0-9547861-0-6, pp 567-573.